

AD-A143 681 ANALYSES ON THE LOW VOLTAGE FREE ELECTRON LASER(U)  
SCHAFFER (W J) ASSOCIATES INC WAKEFIELD MA

1/1

UNCLASSIFIED N00014-80-C-0515

N00014-80-C-0515

F/G 20/5

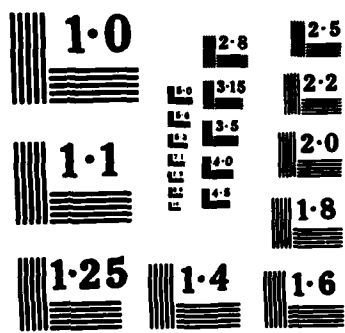
NL

File # 02

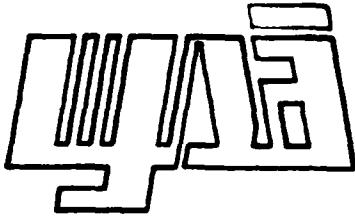
FOLIO 104 D

ping





2



WJSA-FTR-84-19

ANALYSES ON  
THE LOW VOLTAGE FREE ELECTRON LASER

BY

S. A. MANI, J. M. YODER, J. BLIMMEL

JULY 1984

CONTRACT NO. N00014-80-C-0515

PREPARED FOR:

PCO - OFFICE OF NAVAL RESEARCH  
DEPARTMENT OF THE NAVY  
800 N. QUINCY STREET  
ARLINGTON, VA 22217

PREPARED BY:

W. J. SCHAFER ASSOCIATES, INC.  
CORPORATE PLACE 128  
BUILDING 2, SUITE 300  
WAKEFIELD, MASSACHUSETTS 01880

AD-A143 681

DTIC FILE COPY

DTIC  
ELECTE  
JUL 23 1984  
S D E

This document has been approved  
for public release and sale; its  
distribution is unlimited.

84 7 20 080

WJSA-FTR-84-19

ANALYSES ON  
THE LOW VOLTAGE FREE ELECTRON LASER

BY

S. A. MANI, J. M. YODER, J. BLIMMEL

JULY 1984

CONTRACT NO. N00014-80-C-0515

PREPARED FOR:

PCO - OFFICE OF NAVAL RESEARCH  
DEPARTMENT OF THE NAVY  
800 N. QUINCY STREET  
ARLINGTON, VA 22217

PREPARED BY:

W. J. SCHAFER ASSOCIATES, INC.  
CORPORATE PLACE 128  
BUILDING 2, SUITE 300  
WAKEFIELD, MASSACHUSETTS 01880

Accession For	
NTIS GRA&I	<input checked="" type="checkbox"/>
DTIC TAB	<input type="checkbox"/>
Unannounced	<input type="checkbox"/>
Justification	
By _____	
Distribution/	
Availability Codes	
Dist	Avail and/or Special
A-1	

This document has been approved  
for public release and sale; its  
distribution is unlimited.

UNCLASSIFIED

SECURITY CLASSIFICATION OF THIS PAGE

REPORT DOCUMENTATION PAGE				
1a. REPORT SECURITY CLASSIFICATION <b>UNCLASSIFIED</b>		1b. RESTRICTIVE MARKINGS		
2a. SECURITY CLASSIFICATION AUTHORITY		3. DISTRIBUTION/AVAILABILITY OF REPORT  Unclassified/Unlimited		
2b. DECLASSIFICATION/DOWNGRADING SCHEDULE				
4. PERFORMING ORGANIZATION REPORT NUMBER(S) WJSA-FTR-84-19		5. MONITORING ORGANIZATION REPORT NUMBER(S)		
6a. NAME OF PERFORMING ORGANIZATION W.J. Schafer Associates	6b. OFFICE SYMBOL (if applicable) WJSA	7a. NAME OF MONITORING ORGANIZATION Office of Naval Research		
6c. ADDRESS (City, State and ZIP Code) Corporate Place 128 Building 2, Suite 300 Wakefield, MA 01860		7b. ADDRESS (City, State and ZIP Code) 1030 E. Green Street Pasadena, CA		
8a. NAME OF FUNDING/SPONSORING ORGANIZATION Office of Naval Research	8b. OFFICE SYMBOL (if applicable) ONR	9. PROCUREMENT INSTRUMENT IDENTIFICATION NUMBER Contract No. N00014-80-C-0515		
8c. ADDRESS (City, State and ZIP Code) 800 N. Quincy Street Arlington, VA 22217		10. SOURCE OF FUNDING NOS.		
		PROGRAM ELEMENT NO.	PROJECT NO.	TASK NO.
				WORK UNIT NO.
11. TITLE (Include Security Classification) Analysis on The Low Voltage Free Electron Laser				
12. PERSONAL AUTHOR(S) S. A. Mani, J. Yoder, and J. Blimmel				
13a. TYPE OF REPORT Final		13b. TIME COVERED FROM 10/82 TO 7/84		14. DATE OF REPORT - Yr. Mo. Day 1984 - 7 - 16
15. PAGE COUNT 36				
16. SUPPLEMENTARY NOTATION				
17. COSATI CODES			18. SUBJECT TERMS (Continue on reverse if necessary and identify by block number)	
FIELD	GROUP	SUB. GR.		
			Free electron laser (FEL)	
19. ABSTRACT (Continue on reverse if necessary and identify by block number) → The results of calculations on the two stage FEL are presented. Methods to reduce mirror losses at mm wavelengths are suggested. Dielectric stack with teflon and air seem to be the optimum choice to reduce absorption loss. Several methods to maintain a single longitudinal mode operation of the first stage of a two stage FEL are suggested. Finally, the design issues concerned with applying axial electric field by induction to enhance FEL extraction efficiency are discussed. ↖				
20. DISTRIBUTION/AVAILABILITY OF ABSTRACT UNCLASSIFIED/UNLIMITED <input checked="" type="checkbox"/> SAME AS RPT. <input type="checkbox"/> OTIC USERS <input type="checkbox"/>			21. ABSTRACT SECURITY CLASSIFICATION UNCLASSIFIED	
22a. NAME OF RESPONSIBLE INDIVIDUAL Dr. Siva A. Mani		22b. TELEPHONE NUMBER (Include Area Code) 617-246-0450		22c. OFFICE SYMBOL

DD FORM 1473, 83 APR

EDITION OF 1 JAN 73 IS OBSOLETE.

UNCLASSIFIED

SECURITY CLASSIFICATION OF THIS PAGE

## TABLE OF CONTENTS

	<u>PAGE</u>
I. INTRODUCTION	1
II. SECOND STAGE FEL PERFORMANCE	2
III. DIELECTRIC COATINGS	9
IV. GRAZING INCIDENCE OPTICS	18
V. MODE SUPPRESSION TECHNIQUES	20
VI. AXIAL FIELD GRADIENT BY INDUCTION	29
VII. REFERENCES	35

LIST OF TABLES

<u>TABLE NO.</u>	<u>TITLE</u>	<u>PAGE</u>
I	Optical Properties of PTFE (from Ref. 8)	15
II	Calculated Thicknesses of a 20 Layer Teflon for Maximum Reflectivity at 3 mm	17
III	Number of Longitudinal Modes in a Gain Line Width for Several Frequencies and Resonator Lengths	20
IV	The Predicted Properties of Various Core Materials and Geometries for Several Pulse Durations (from Ref. 13)	34



# LIST OF FIGURES

<u>FIGURE NO.</u>	<u>TITLE</u>	<u>PAGE</u>
1	Second Stage Extraction Efficiency vs $a_{so}$ $a_{po}$ . Axial electrical field is applied to enhance extraction efficiency	5
2	Effect of Energy Spread on Extraction Efficiency	6
3	Effect of Energy Spread on Extraction Efficiency	7
4	Effect of Energy Spread on Extraction Spread	8
5	Refractive Index vs. Wave number in the mm Wave Region for Different Low Loss Polymers (from Ref. 8)	13
6	Absorption Coefficient vs. Wave number in the mm Wave Region for Different Low Loss Polymers (from Ref. 8)	14
7	Mode Selection Through Use of an Additional Intra Cavity Low Bandwidth Gain Medium	23
8	FEL Operation with an Additional Narrow Bandwidth Gain Region	24
9	Injection Locking of FEL Cavity	24
10	Use of a Fabry-Perot Etalon for SLM Selections	25
11	Transmission of a Fabry-Perot Etalon	25
12	Reflection Echelon Used at Littrow Angle	28
13	Echelon Used for FEL	28
14	Practical Field Gradients that can be Obtained Using Metglass Core (from Ref. 13)	31
15	Energy Dissipation in Different Core Materials (from Ref. 13)	32

## I. INTRODUCTION

Over the past four years, WJSA has contributed significantly to the two-stage free electron laser program carried out by the Office of Naval Research.<sup>1-3</sup> Our studies have concentrated on decreasing the first stage cavity losses, optimal design of the two stage free electron laser that uses a single electron beam and on detailed calculations of the dynamics of the FEL intersection.

In this report, we present results of calculations on the performance of the second stage of the two stage free electron laser, dielectric coatings to decrease the absorption losses, analysis on the use of grazing angle incidence optics and methods to suppress unwanted modes in the first stage. We have found that the first stage cavity losses can be decreased by a factor of 3 to 5 from that of the bare metal by a dielectric stack that consists of teflon and air. We propose to carry out a bench top experiment to verify this concept. We find that the grazing angle incidence optics will not reduce the cavity losses from that of the normal incidence optics, but may result in compact cavities. We present several methods to maintain a single longitudinal mode operation of the first stage of a two stage free electron laser. Finally, we discuss some of the design issues concerned with applied and axial electric field by induction to enhance the extraction efficiency of the FEL operating with an electromagnetic pump.

## II. SECOND STAGE FEL PERFORMANCE

In the previous report, we described computations leading to the first stage performance of a two stage FEL. The programs that we have developed enable one to calculate the steady state transverse mode structures of the first stage output in a stable cavity configuration. The calculations are valid for small single pass gain (typically <10%). In the steady state operation of the two stage FEL, the first stage output is not coupled to outside and the gain in the first stage has to equal the losses in the optical system. Typical losses are expected to be less than 1% and thus the saturated gain of the first stage will be less than 1%. Our finding in this situation is that the cavity tends to choose the lowest order mode of the bare resonator with the relative amplitudes of higher order modes being very small. As a first approximation, one can then take the transverse mode of the electromagnetic pump to be gaussian. In this section, we briefly describe the calculations performed to evaluate the second stage FEL performance.

The analysis carried out by us is strictly one dimensional but with some of the two dimensional effects included. For example, we take into account the phase variation of the pump wave with respect to  $z$ , the propagation direction, due to beam divergence.

We assume the pump wave and second stage output waves to be described by vector potentials  $\vec{A}_p$  and  $\vec{A}_s$  respectively. These are given by

$$\vec{A}_p = \hat{x} \sqrt{2} \left( \frac{mc^2}{e} \right) a_p(z) \sin(\theta_p + \omega_p t + \phi_p) \quad (1)$$

and

$$\vec{A}_s = \hat{x} \sqrt{2} \left( \frac{mc^2}{e} \right) a_s(z) \sin(\Theta_s - \omega_s t + \phi_s) \quad (2)$$

where

$$\Theta_p = \int k_p dz = k_{po} z + \frac{k_{po} (x^2 + y^2)}{[1 + (z_R/z)^2]} - (m+n+1) \tan^{-1}(z/z_R) \quad (3)$$

for the  $TE_{(m,n)}$  mode of the pump. In what follows, we shall consider only  $m=n=0$  case, but the generalization to multiple pump modes is straightforward. Here  $k_{po}$  ( $= 2\pi/\lambda_p$ ) is the free space wave number of the pump wave and  $z_R$  is the Rayleigh range of the pump beam and is equal to  $\pi \omega_o^2/\lambda_p$  where  $\omega_o$  is the beam waist radius and  $\lambda_p$  is the pump wavelength. The definition for  $\Theta_s$  is similar to  $\Theta_p$ ; however, since the wavelength of the output radiation is much less than that of the pump, the terms in  $\Theta_s$  corresponding to the second and third of (3) may be neglected giving  $\Theta_s \approx k_{so} z$ . We shall assume that there is also a scalar potential  $\phi(z)$  giving rise to an axial electric field  $-\nabla\phi$ . The energy equation is

$$\frac{d\gamma}{dt} = \frac{e}{mc} (\vec{\beta} \cdot \vec{E}) \quad (4)$$

where  $c\vec{\beta}$  is the velocity of the electron. Converting the independent variable  $t$  to  $z$ , we have,

$$\begin{aligned} \frac{d\gamma}{dz} = & - \frac{(\omega_s - \omega_p)}{c\beta_z \gamma} a_s a_p \sin \psi - \left( \frac{e}{mc^2} \right) \frac{\partial \phi}{\partial z} \\ & - \frac{\epsilon}{\gamma c \beta_z} \{ \omega_s a_s^2 \sin 2\theta - \omega_p a_p^2 \sin (2\psi - 2\theta) \\ & + (\omega_s + \omega_p) a_s a_p \sin (\psi - 2\theta) \} \end{aligned} \quad (5)$$

$$\frac{d\psi}{dz} = (k_s + k_p) - \frac{(\omega_s - \omega_p)}{c\beta_z} \quad (6)$$

where  $\epsilon = 1$  for linearly polarized light. For circularly polarized light (Eqs. (1) and (2) have to be suitably modified for this case)  $\epsilon$  will be equal to zero. The term containing  $\epsilon$  is a rapidly oscillating term and may be neglected.  $\psi$  is the relative phase of the electron with respect to the output wave. The parallel velocity  $c\beta_z$  in Eq. (6) may be written in terms of the total beam energy and the pump and output vector potentials as

$$c\beta_z = c \left\{ 1 - \frac{1 + \alpha^2}{\gamma^2} \right\}^{1/2} \quad (7)$$

where

$$\begin{aligned} \alpha^2 = & (a_p^2 + a_s^2 - 2 a_p a_s \cos \psi) + \epsilon \{ 2 a_p a_s \cos (\psi - 2\phi) \\ & - a_p^2 \cos (2\psi - 2\phi) - a_s^2 \cos 2\phi \} \end{aligned} \quad (8)$$

Equations (5) and (6) are solved for different initial conditions in  $\psi$  and  $\gamma$ . The energy loss by the electrons is then averaged over the initial distribution function in  $\gamma$  and  $\psi$ .

Sample results from the computer runs are shown in Figures 1 to 4. Figure 1 shows the extraction efficiency as a function of the product of the vector potential as  $a_{so} a_{po}$ . Also shown are the accelerating fields necessary to achieve the efficiency enhancement. With electromagnetic pump of wavelength  $< 1 \text{ mm}$ , the maximum practical value for  $a_{so} a_{po}$  is  $\sim 3 \times 10^{-5}$ . Figure 1 was plotted assuming mono-energetic, zero emittance electron beam. The effect of energy spread or extraction efficiency is shown in Figures 2 to 4. The higher the product  $a_{so} a_{po}$ , the greater is the ponderomotive potential well depth and hence the greater can be the energy spread of the incident electron beam. Since the accelerating field is equivalent to tapering the wiggler, the curves for extraction efficiency are not symmetrical about  $(\Delta\gamma/\gamma) = 0$ .

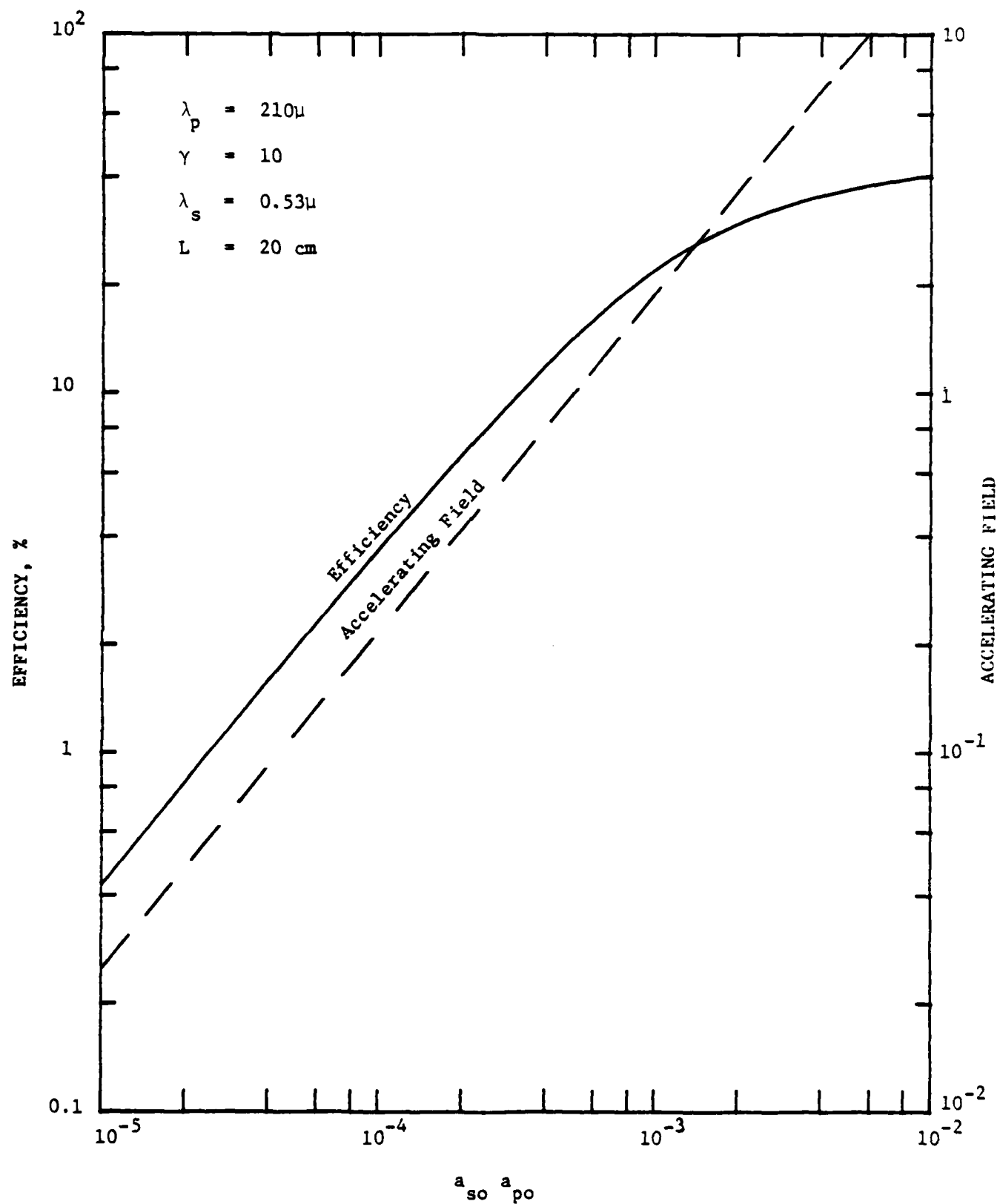


Figure 1. Second Stage Extraction Efficiency vs.  $a_{so} a_{po}$ . Axial electric field is applied to enhance extraction efficiency.

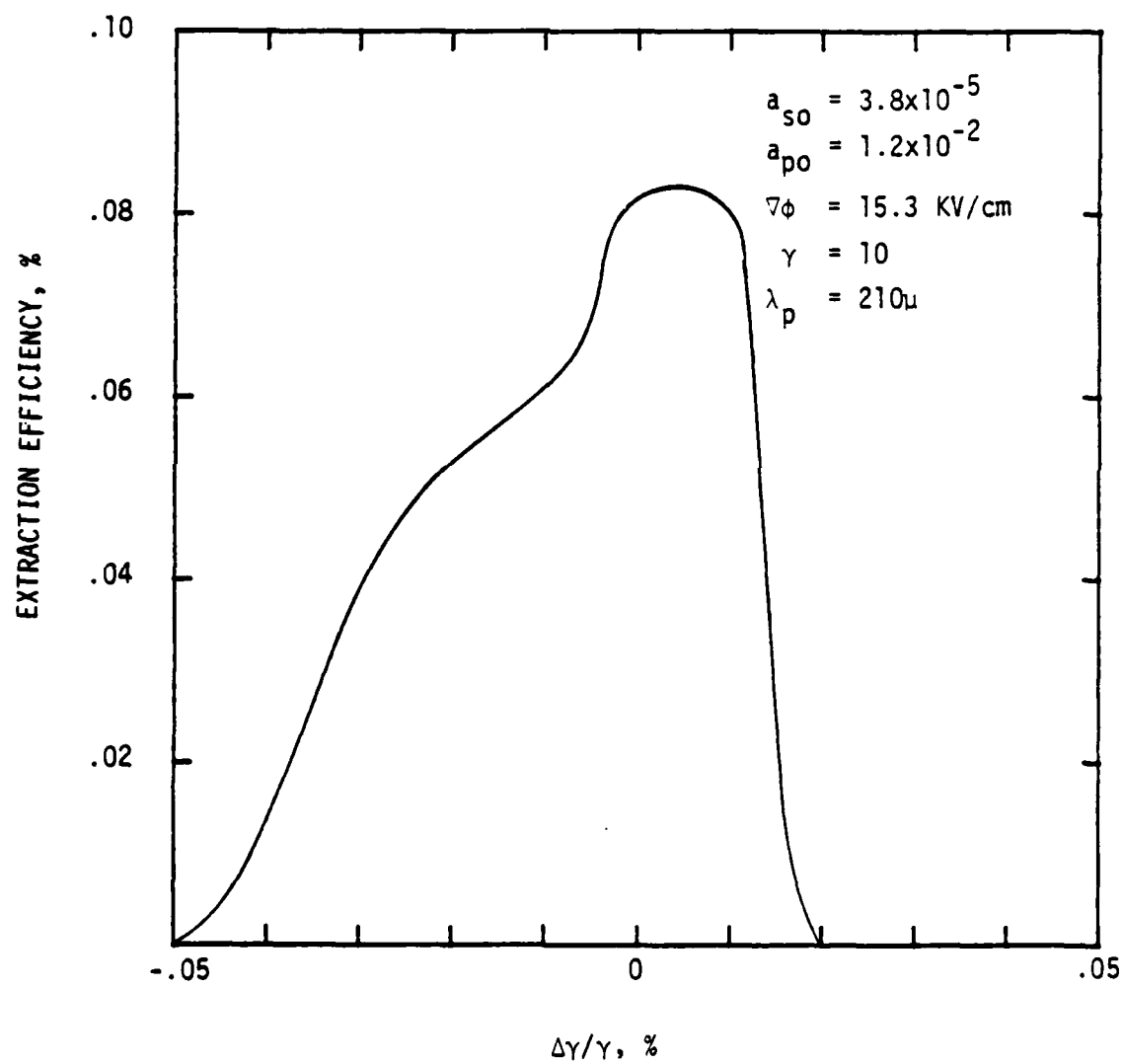


Figure 2. Effect of Energy Spread on Extraction Efficiency

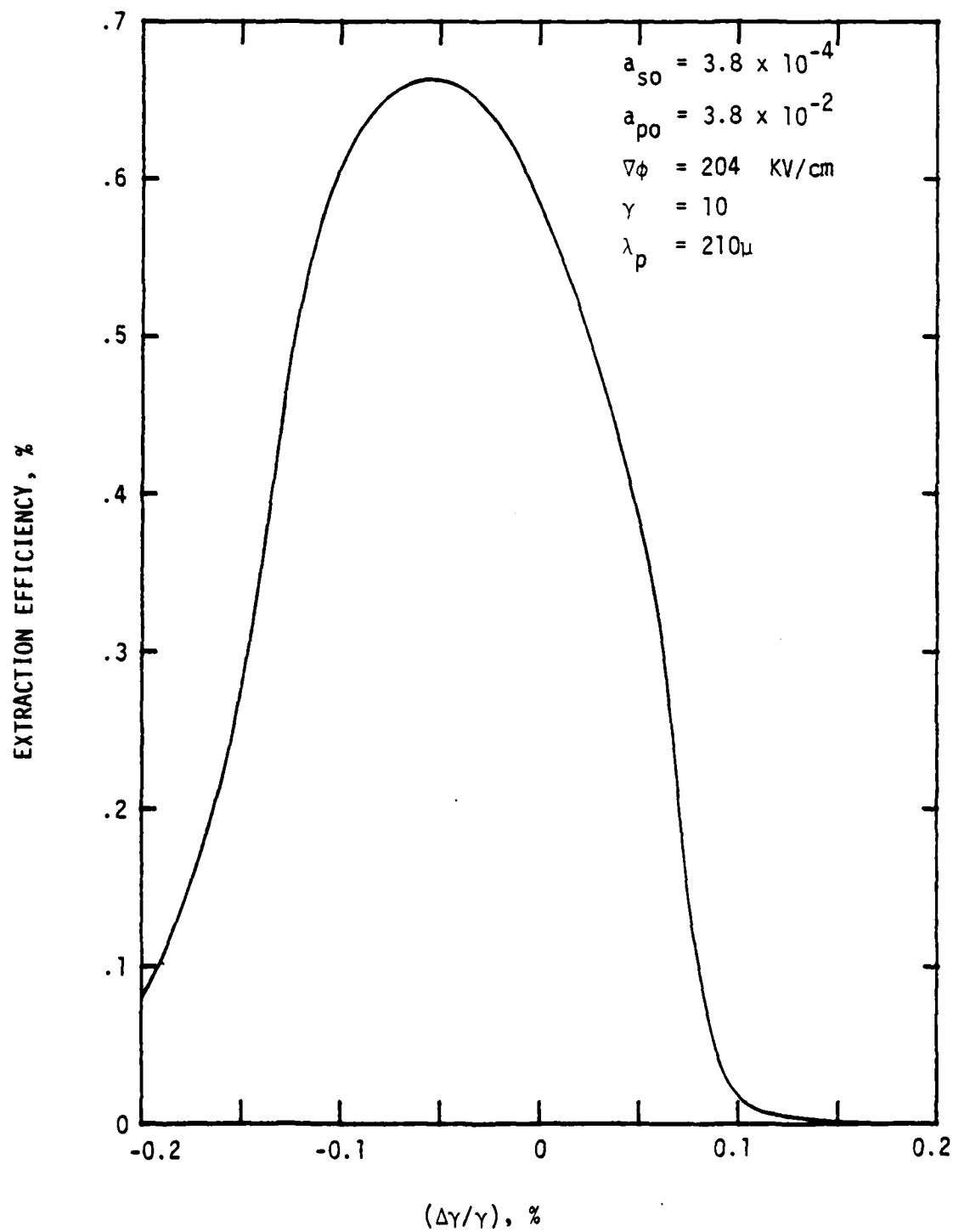


Figure 3. Effect of Energy Spread on Extraction Efficiency



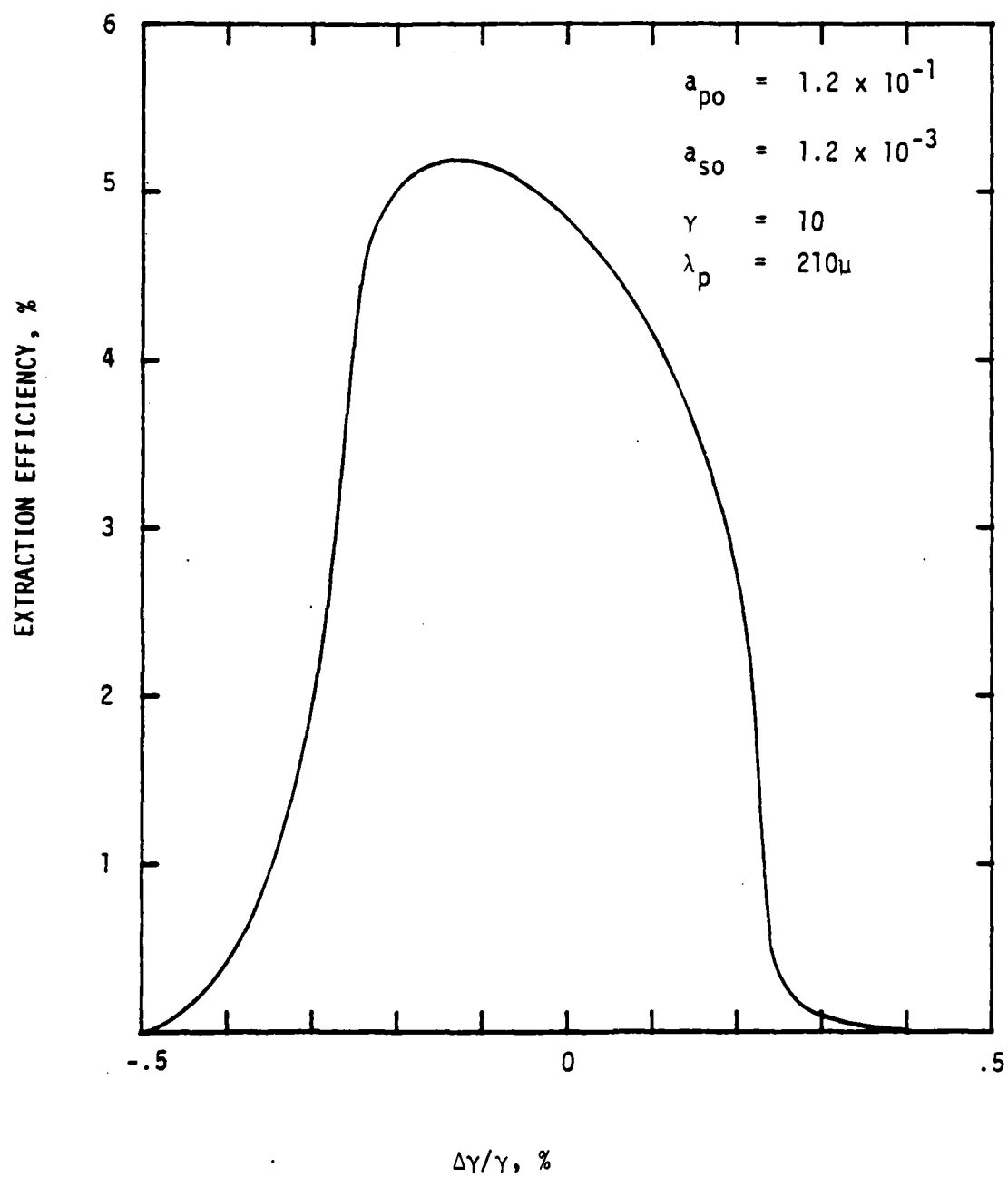


Figure 4. Effect of Energy Spread on Extraction Efficiency

### III. DIELECTRIC COATINGS

In the visible and near infrared wavelength region, the dielectric quarter-wave multi-layer reflector is widely used in situations requiring especially high reflectance. The dielectric reflector is made from materials that have minimal absorption, and the coating consists of alternate layers of low- and high-index materials. For maximum reflectance at a particular wavelength, the optical thickness of each layer is chosen to be one quarter of that wavelength. In the absence of absorption and scattering, the reflectance of a quarter-wave stack may be made to approach cavity by adding sufficient number of alternate layers of high- and low-index materials. In practice, however, small amounts of absorption in the coating materials place an upper limit on the reflectance that can be achieved with a quarter-wave stack.

Carniglia and Apfel<sup>4</sup> have recently shown theoretically that for two coating materials of different absorption coefficients, the optimum thickness of the coatings is not a quarter wave stack. They have solved the problem of finding the thicknesses of the optimum pair of layers that give maximum final reflectance as a substrate or a system of layers having a given reflectance. Starting from a given substrate, one can progressively design the optimum pairs. One of the principal conclusions of Carniglia and Apfel is that the limiting reflectance of a reflector constructed out of optimum pairs approaches unity if one of the coating materials is not absorbing.

We reproduce below a brief review of the dielectric coatings given by Carniglia and Apfel.

"A quarter-wave stack multilayer reflector is made using two dielectric materials having different refractive indices. These two materials are coated or deposited alternately in layers on a substrate. The high reflective index  $n_H$  and the low refractive index  $n_L$  may be written in the form

$$n_H = n_1 - ik_1, \quad (9a)$$

$$n_L = n_2 - ik_2, \quad (9b)$$

where  $n_1$  and  $n_2$  are the real parts of  $n_H$  and  $n_L$  respectively, and  $k_1$  and  $k_2$  are the corresponding imaginary parts or absorption coefficients. For dielectric materials, the value of  $k/n$  is small ( $\ll 1$ ) and often is assumed to be zero. The thickness  $d$  of each layer in a quarter-wave stack is chosen so that the optical thickness  $nd$  of the layer is equal to  $\lambda_0/4$  where  $\lambda_0$  is the design wavelength.

To achieve the greatest reflectance, the outer layer of a quarter-wave stack should generally be of the high-index material. If the substrate is a low-index dielectric material, the layer adjacent to the substrate should also be of the high-index material leading to an odd number of layers in the design. In the absence of absorption ( $k_1 = k_2 = 0$ ), the amplitude reflectance  $r$  of a quarter-wave stack may be written

$$r = (n_o - n_e)/(n_o + n_e), \quad (10)$$

where  $n_o$  is the refractive index of the incident medium and  $n_e$  is an equivalent index of the reflector taken as a whole. For an odd number of layers  $l$ , the equivalent index is

$$n_e = (n_H)^{l+1} (n_L)^{l-1} n_s^{-1}, \quad (11)$$

where  $n_s$  is the (real) index of the substrate. Notice that usually  $n_e > n_o$ , and  $r$  is negative. This corresponds to a phase shift of  $\pi$  for the reflected wave. The intensity reflectance or radiant reflectance  $R$  is the absolute square of the amplitude reflectance  $r$ . As the number of layers increases,  $n_e$  becomes larger and  $R$  approaches asymptotically to unity.

An alternate description of the reflective properties of a quarter wave stack is in terms of the standing wave ratio (SWR), or voltage standing wave ratio as it is called in microwave theory. The SWR is defined to be the ratio of the maximum to minimum electric field amplitude in the standing wave formed by the interference of the incident and reflected waves.<sup>5</sup> The SWR may be expressed in terms of the radiant reflectance using

$$\text{SWR} = (1 + \sqrt{R}) / (1 - \sqrt{R}). \quad (12)$$

For the nonabsorbing quarter-wave stack with an odd number of layers  $2l$  discussed above, it can be shown that

$$\text{SWR} = n_e / n_o = (n_H)^{1+l} (n_L)^{1-l} (n_o n_s)^{-1} \quad (13)$$

If one or both of the materials has non-negligible absorption, the SWR saturates at a value corresponding to the limit predicted by Koppelman<sup>6</sup> for a quarter-wave stack. Expressed in terms of the maximum radiant reflectance, this limit is

$$R_k = 1 - 2\Delta_k, \quad (14)$$

where

$$\Delta_k = \pi n_o (k_1 + k_2) / (n_1^2 - n_2^2) \quad (15)$$

Here  $n_o$  is the refractive index of the incident medium, and the subscripts 1 and 2 refer to the high- and low-index materials, respectively, as in Eq. (9).

At this point, the concept of an optimum pair (OP) can be introduced: It can be shown that after the Koppelman limit to the reflectance is reached, the effect of adding another pair of low- and high-index layers is negligible. However, if the thicknesses of the layers are not constrained to be equal to quarterwaves, then the Koppelman limit can be exceeded. The optimum thicknesses for an added pair of

layers can be found by adding a low-index layer and a high-index layer to the saturated quarter-wave stack, and letting the optical thicknesses of these two layers each range over the values 0 to 2 quarter waves. The optimum pair of layers is defined as having the combination of thicknesses resulting in the highest reflectance."

It seems that one could reduce the absorption of the mirror from that of the Koppelman limit by a factor of 5 to 10 in practice. The problem then is one of finding suitable dielectric materials that have very low absorption in the millimeter wavelength region. We have carried out some literature search on the optical properties of the dielectrics in the millimeter wavelength region. An excellent source of bibliography on the research carried out in the millimeter wavelength region is the paper by Simonis.<sup>7</sup> The work of Birch, Dromey and Lesurf<sup>8</sup> indicate the possibility of using low-loss polymers as the dielectric materials. Among the common polymers studied by these authors, polytetrafluoroethylene (PTFE or teflon) seems to have the lowest absorption coefficient in the wavelength region of 1 to 3 mm. Figures 5, 6, and Table 1 reproduced from Ref. 8 show the refractive index of the several low-loss polymers. Since the wavelength of interest is 1 to 3 mm, it is possible to use air (or vacuum) as the low refractive index dielectric layer and teflon as the high index material; the stack would consist of a series of sheets of teflon separated by the proper amount and placed in front of the metal mirror. Since dry air has negligible absorption at these wavelengths, one could reduce the losses of the stack by a factor of 3 to 5 as compared to that of the bare metal. The sheets of teflon could be supported at

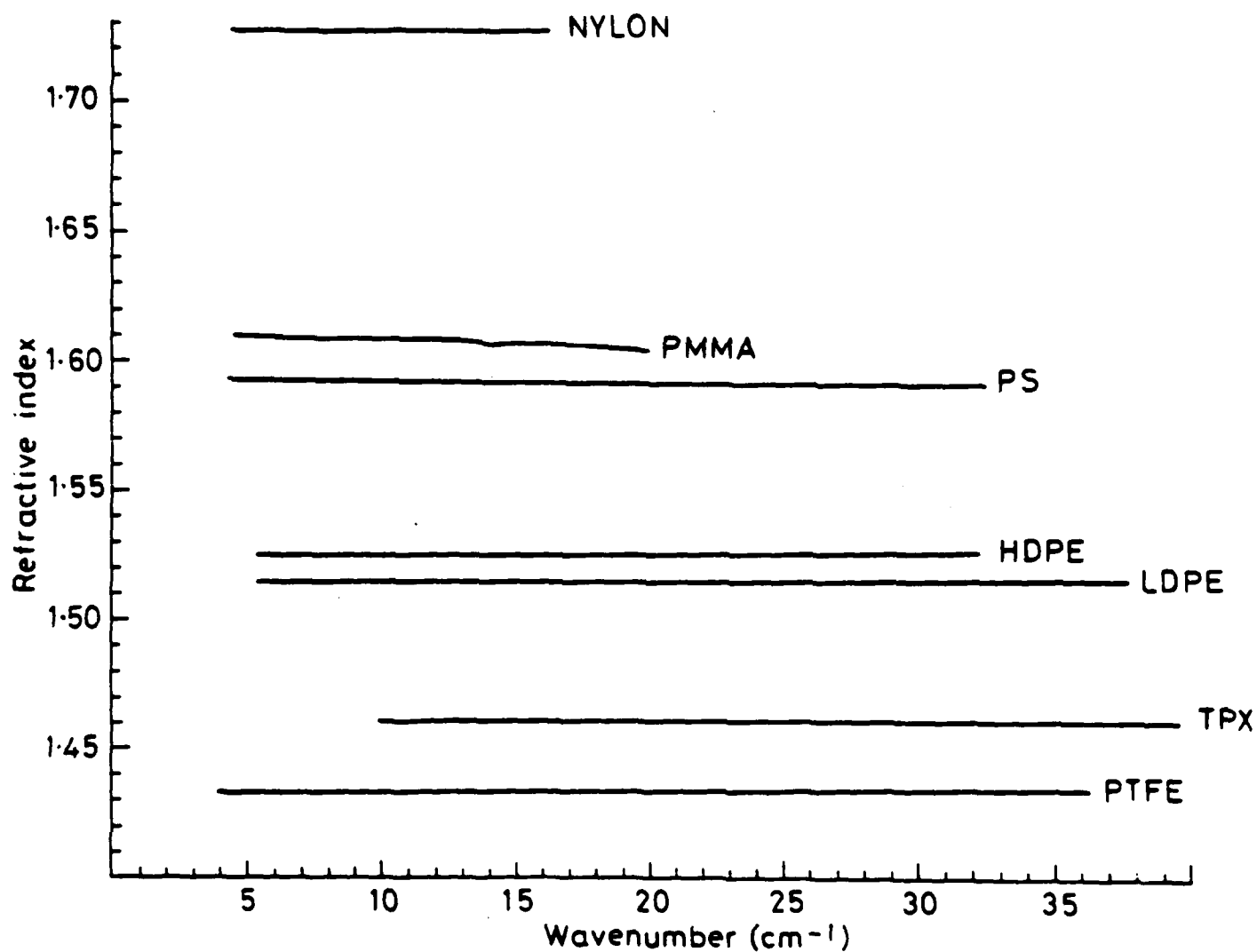


Figure 5. Refractive Index vs. Wave number in the mm Wave Region for Different Low Loss Polymers (from Ref. 5)

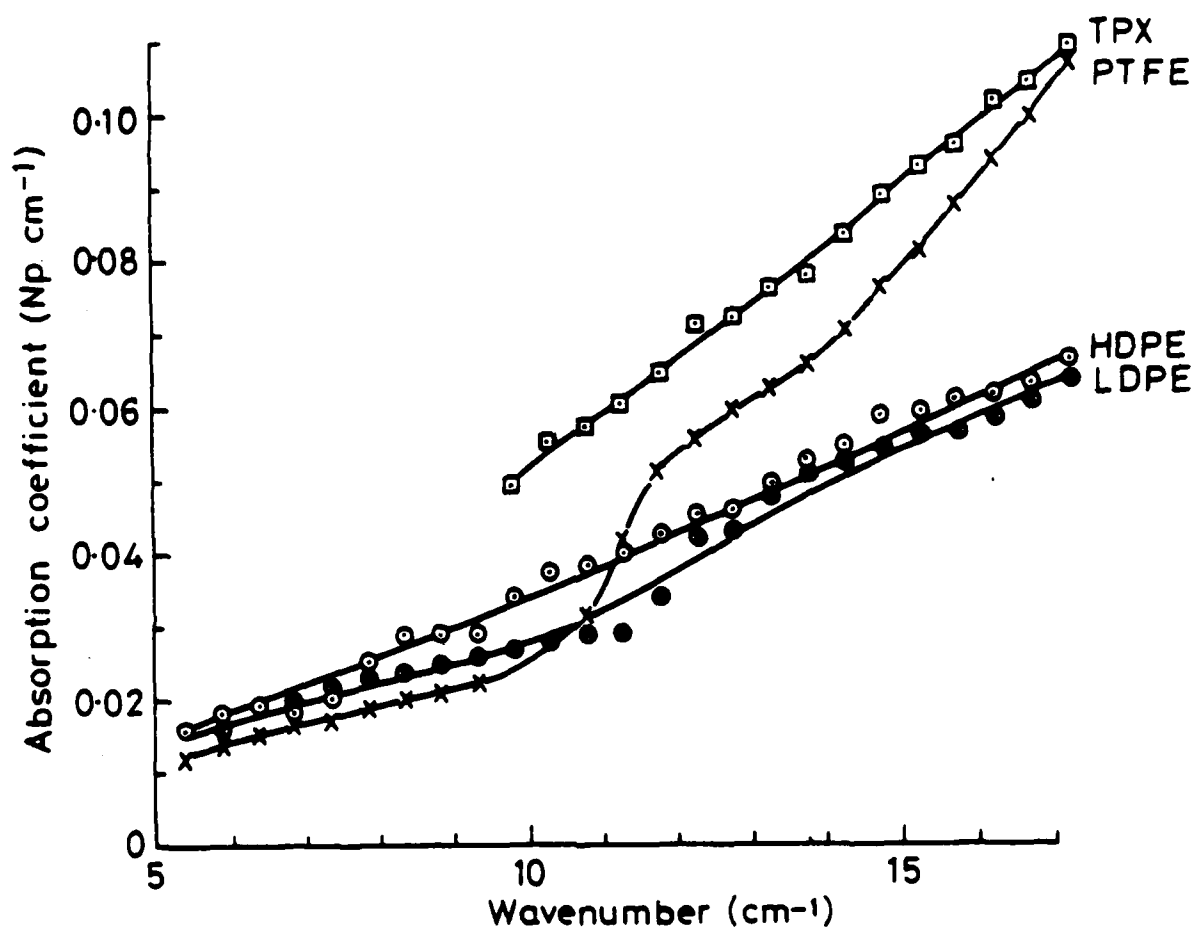


Figure 6. Absorption Coefficient vs. Wave number in the mm Wave Region for Different Low Loss Polymers (from Ref. 3)

TABLE I. OPTICAL PROPERTIES OF PTFE (From Ref. 6)

waveno. (cm <sup>-1</sup> )	Freq. (GHz)	n	Abs. Coef. (Np.cm <sup>-1</sup> )	$\xi'$	$\xi''$	Loss tangent
5.37	161.0	1.43295	0.012	2.05334	.00051	.00025
5.86	175.7	1.43323	0.014	2.05415	.00055	.00027
6.35	190.3	1.43324	0.015	2.05419	.00055	.00027
6.84	204.9	1.43323	0.017	2.05415	.00055	.00027
7.32	219.6	1.43323	0.017	2.05414	.00054	.00026
7.81	234.2	1.43303	0.019	2.05358	.00055	.00027
8.30	248.9	1.43293	0.020	2.05327	.00056	.00027
8.79	263.5	1.43295	0.021	2.05334	.00056	.00027
9.28	278.1	1.43294	0.022	2.05331	.00055	.00027
9.77	292.8	1.43290	0.027	2.05321	.00064	.00031
10.25	307.4	1.43293	0.028	2.05329	.00063	.00031
10.74	322.0	1.43295	0.032	2.05335	.00067	.00033
11.23	336.7	1.43290	0.042	2.05321	.00085	.00041
11.72	351.3	1.43290	0.051	2.05319	.00098	.00048
12.21	366.0	1.43295	0.055	2.05336	.00103	.00050
12.70	380.6	1.43298	0.059	2.05343	.00107	.00052
13.18	395.2	1.43291	0.062	2.05323	.00108	.00052
13.67	409.9	1.43291	0.065	2.05322	.00108	.00053
14.16	424.5	1.43290	0.070	2.05321	.00113	.00055
14.65	439.2	1.43288	0.076	2.05315	.00118	.00058
15.14	453.8	1.43289	0.081	2.05317	.00123	.00060
15.63	468.4	1.43290	0.087	2.05321	.00127	.00062
16.11	483.1	1.43287	0.093	2.05313	.00131	.00064
16.60	497.7	1.43286	0.099	2.05309	.00136	.00066
17.09	512.3	1.43288	0.106	2.05316	.00141	.00069
17.58	527.0	1.43288	0.110	2.05314	.00143	.00070
18.07	541.6	1.43286	0.111	2.05310	.00140	.00068
18.55	556.3	1.43287	0.113	2.05312	.00139	.00068
19.04	570.9	1.43290	0.121	2.05319	.00145	.00071
19.53	585.5	1.43290	0.129	2.05320	.00151	.00073
20.02	600.2	1.43290	0.134	2.05319	.00153	.00074
20.51	614.8	1.43292	0.140	2.05325	.00155	.00076
21.00	629.5	1.43294	0.146	2.05331	.00159	.00077
21.48	644.1	1.43295	0.154	2.05335	.00164	.00080
21.97	658.7	1.43296	0.163	2.05338	.00169	.00082
22.46	673.4	1.43297	0.171	2.05341	.00174	.00085
22.95	688.0	1.43298	0.178	2.05343	.00176	.00086
23.44	702.6	1.43299	0.184	2.05347	.00179	.00087
23.93	717.3	1.43301	0.193	2.05351	.00184	.00089
24.41	731.9	1.43303	0.203	2.05357	.00190	.00092
24.90	746.6	1.43304	0.211	2.05361	.00193	.00094
25.39	761.2	1.43306	0.221	2.05365	.00199	.00097
25.88	775.8	1.43307	0.232	2.05370	.00205	.00100
26.37	790.5	1.43309	0.243	2.05375	.00210	.00102
26.86	805.1	1.43311	0.256	2.05380	.00218	.00106
27.34	819.7	1.43313	0.272	2.05385	.00227	.00110
27.83	834.4	1.43314	0.287	2.05389	.00235	.00115
28.32	849.0	1.43315	0.305	2.05392	.00245	.00119
28.81	863.7	1.43316	0.323	2.05395	.00255	.00124
29.30	878.3	1.43315	0.342	2.05393	.00266	.00130
29.79	892.9	1.43312	0.362	2.05382	.00277	.00135
30.27	907.6	1.43308	0.383	2.05373	.00289	.00141
30.76	922.2	1.43305	0.403	2.05363	.00299	.00145
31.25	936.9	1.43301	0.418	2.05352	.00305	.00149
31.74	951.5	1.43299	0.429	2.05346	.00309	.00150
32.23	966.1	1.43299	0.438	2.05345	.00310	.00151



places where the incident flux would be very small as well as outside the footprint of the optical beam. Table II shows our calculation for the thickness of teflon and air layers for a 20 layer dielectric stack or copper at a wavelength of 3 mm.

An experiment is proposed to verify this concept to improve the reflectivity.

TABLE II  
CALCULATED THICKNESSES OF A 20 LAYER TEFLON FOR MAXIMUM REFLECTIVITY AT  
3 MM

Substrate Reflectivity = 0.99

No.	Thickness of Layers in mm		Reflectivity
	Teflon	Air	
1	0.509	0.781	0.99475
2	0.495	0.809	0.99707
3	0.472	0.854	0.99821
4	0.441	0.916	0.99876
5	0.406	0.981	0.99904
6	0.377	1.034	0.99918
7	0.355	1.070	0.99925
8	0.342	1.092	0.99929
9	0.333	1.105	0.99932
10	0.328	1.113	0.99933
11	0.325	1.118	0.99934
12	0.323	1.121	0.99934
13	0.322	1.123	0.99935
14	0.321	1.124	0.99935
15	0.321	1.124	0.99935
16	0.321	1.125	0.99935
17	0.320	1.125	0.99935
18	0.320	1.125	0.99935
19	0.320	1.125	0.99935
20	0.320	1.125	0.99935

#### IV. GRAZING INCIDENCE OPTICS

It is well-known that the reflection coefficient of a surface can be increased by increasing the angle of incidence towards  $90^\circ$  for light that is polarized perpendicular to the plane of incidence. For the two-stage FEL concept, it was felt that one could make a higher Q cavity for the electromagnetic pump wave using grazing incidence mirrors. A careful analysis, however shows that this is not the case. In this section, we derive the expression for the reflection coefficient from a grazing incidence mirror and compare the results with a cavity consisting of normal incidence optics.

The complex index of refraction of a metal may be written as

$$\bar{n} = n(1 - i\chi). \quad (16)$$

It is shown in Ref. 9 that for good conductors,  $\chi \approx 1$  and that  $n$  is given by

$$n \approx \frac{c}{\omega\delta} \quad (17)$$

where  $\delta$  is the skin-depth at the frequency  $\omega$ . Using Maxwell's equations, it is straightforward to work out the reflection coefficient at the boundary between metal and vacuum (or air). For electromagnetic wave whose polarization is perpendicular to the plane of incidence, the reflection coefficient is given by<sup>10</sup>

$$R = \frac{(n - \cos I)^2 + n^2 \chi^2}{(n + \cos I)^2 + n^2 \chi^2} \quad (18)$$

where  $I$  is the angle of incidence. For  $I \approx \frac{\pi}{2}$ , writing  $I = \frac{\pi}{2} - \alpha$ , we can rewrite  $R$  as

$$R = 1 - \frac{4n \sin \alpha}{(n + \sin \alpha)^2 + n^2 \chi^2} \quad (19)$$

Loss per surface is therefore given by  $1-R$  and is equal to

$$\frac{4n \sin \alpha}{(n + \sin \alpha)^2 + n^2 \chi^2} \quad (20)$$

At each mirror, the beam is turned by an angle  $2\alpha$ . The minimum number of mirrors required to turn the beam by  $\pi$  radians is  $\frac{\pi}{2\alpha} + 2$ . The two extra mirrors are required to transpose the beam onto itself when  $\alpha \neq \frac{\pi}{2}$ . The total cavity loss with grazing incidence optics (ignoring, diffraction and scattering) is then given by

$$2 \times \frac{4n \sin \alpha}{(n + \sin \alpha)^2 + n^2 \chi^2} \cdot \left( \frac{\pi + 4\alpha}{2\alpha} \right) \quad (21)$$

For normal incidence, the cavity loss per round trip is given by

$$\text{Loss} \Big|_{\text{Normal}} = \frac{2 \times 4n}{(n+1)^2 + n^2 \chi^2} \quad (22)$$

The ratio of the losses for the two cases is given by dividing eq. (21) by eq. (22).

$$\text{Ratio} = \left( \frac{\sin \alpha}{\alpha} \right) \left( \frac{\pi + 4\alpha}{2} \right) \frac{(n+1)^2 + n^2 \chi^2}{(n + \sin \alpha)^2 + n^2 \chi^2} \quad (23)$$

Since  $n \gg 1$  and  $\chi \approx 1$  for good conductors, the ratio approaches  $\frac{\pi}{2}$  as  $\alpha \rightarrow 0$ . We therefore conclude that the cavity losses with grazing incidence optics is larger than the losses with normal incidence optics at least by a factor of  $\frac{\pi}{2}$ .

## V. MODE SUPPRESSION TECHNIQUES

The operating wavelength of the first stage of a free electron laser (FEL) is about 0.3 to 3.0 mm (1000-100 GHz). The laser cavities are typically 3 to 10 meters long. Thus the single longitudinal mode, (SLM), spacing for these cavity lengths (given by  $c/2L$ ) is  $5 \times 10^7$  -  $1.5 \times 10^7$  Hz, respectively. The gain bandwidth of the FEL is approximately 1% which corresponds to 1 to 10 GHz for 100 GHz and 1000 GHz operation, respectively. Thus the number of longitudinal modes in a linewidth is 20 to 200 for a 3M long cavity and 70 to 700 for a 10M long cavity. The lower number in each case is for 100 GHz and the higher number is for 1000 GHz operation. These results are summarized in Table 3.

TABLE III  
NUMBER OF LONGITUDINAL MODES IN A GAIN LINE WIDTH FOR SEVERAL  
FREQUENCIES AND RESONATOR LENGTHS

Frequency/Wavelength	Number of Longitudinal Modes	
	300 cm Cavity	1000 cm Cavity
100 GHz/3mm	20	70
300 GHz/1mm	60	200
1000 GHz/300 $\mu$ m	200	700

The FEL pump wavelength must be single frequency for efficient generation of the FEL output wavelength. Thus, mode selection in the first stage resonant cavity is necessary. Two important requirements on the mode selection technique are that it must be capable of handling very high fluences ( $100\text{--}1000\text{ J/cm}^2$  for  $10\mu$  seconds,  $10^7\text{--}10^8\text{ w/cm}^2$  flux) and that the cavity be a very low loss (less than 0.001 fractional loss, preferably  $\sim 10^{-4}$  fractional loss per pass).

The following is a list of the general methods of obtaining a single longitudinal mode in laser cavities.

1. Use of a short cavity so that only one longitudinal mode (spacing  $\Delta\nu = c/2L$ ) is within the gain linewidth.
2. Low operating pressures (for gas lasers) so that the gain linewidth is very narrow. For FEL's the analogue is operation with very very long wiggler section.
3. Operation of a master oscillator power amplifier, MOPA, so that a short and/or low power resonant cavity is used to generate low power SLM radiation and a larger cavity is used to generate the high power beam.
4. Frequency stabilization of a resonant cavity by injection locking with a SLM frequency.
5. Use of a Fabry-Perot etalon to select a single longitudinal mode.
6. Use of a high resolution grating as one of the laser cavity mirrors.

To obtain SLM operation with method 1 (very short cavity) would require a 15 cm cavity at 100 GHz and a 1.5 cm cavity at 1000 GHz.

This would obviously be impractical and would leave insufficient gain length.

Method 2 (very low bandwidth gain medium) fails since a narrower gain linewidth than  $\sim 1\%$  is not achievable without extremely long wiggler regions and very uniform electron beams.

A variation of method 2 is mode selection by creation of additional gain for a single desired mode. This is shown schematically in Figure 7. This can be done in gas lasers by making the low gain region a very low pressure discharge.<sup>11</sup> The analogue in FEL's is to have a second, narrow bandwidth gain section which may or may not be a FEL. Non-FEL sources may be gas masers. These will require a window to separate them from the high vacuum FEL. Schematically this is shown in Figure 8 in the form of a ring resonator. The grazing incidence expansion mirrors are used to reduce the flux on the windows and other mirrors in the optical system.

The third method, MOPA, is not suited to the two stage FEL since a very high power resonant cavity is required. A variation which may be suited is method four which is shown in Figure 9. An external SLM source is injected into a resonant cavity to lock the frequency to a single value. This technique has been used by a number of investigators to mode select TEA CO<sub>2</sub> lasers.<sup>12</sup> Only a few watts of injected power are required to obtain megawatts of SLM output power. Although very effective for pulsed lasers, we do not know how effective it would be locking CW lasers.

Method five is the use of a Fabry-Perot etalon to select out a preferred longitudinal mode. A schematic diagram is shown in Figure 10. The transmission of the Fabry-Perot etalon is shown schematically

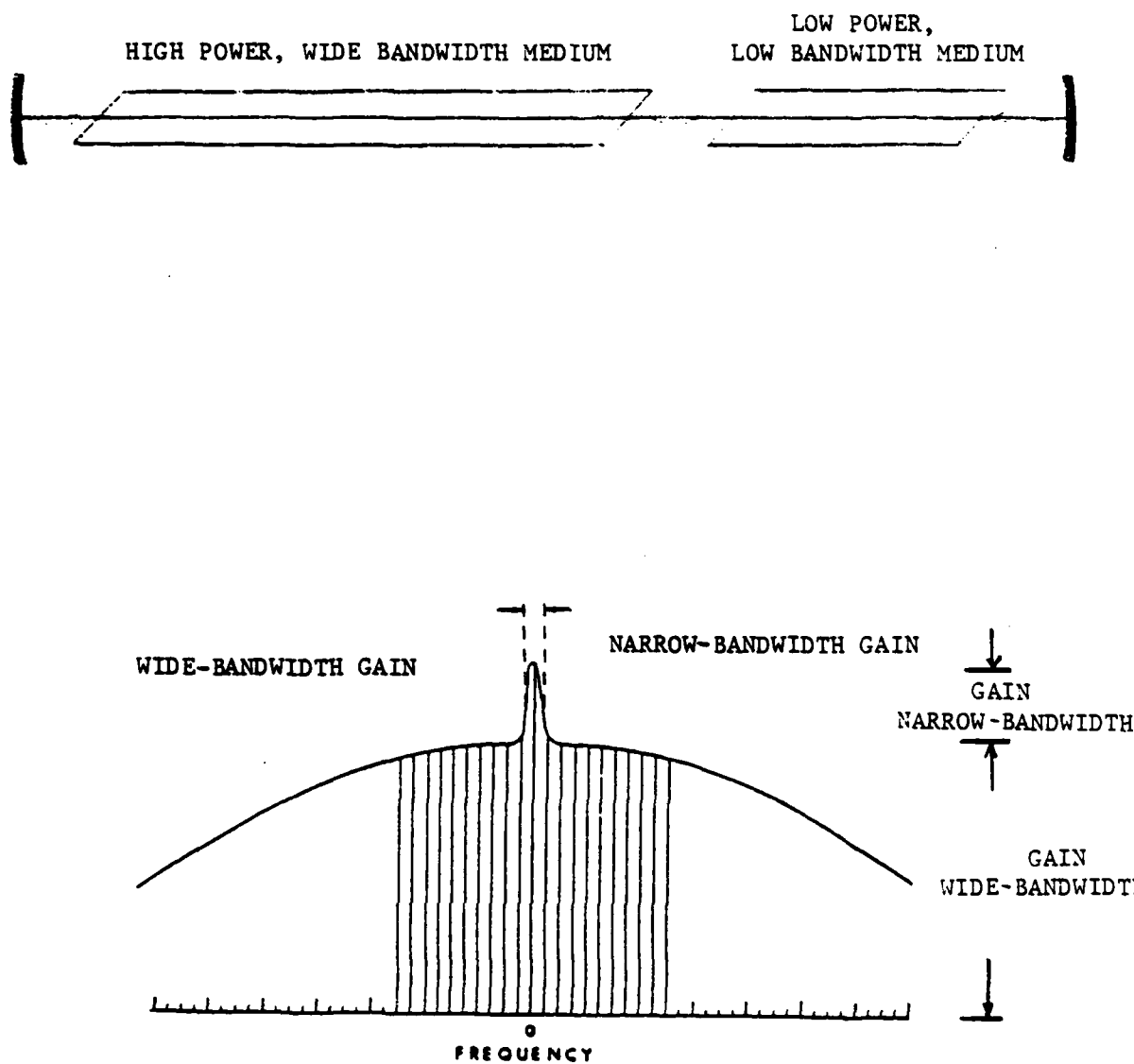


Figure 7. Mode Selection Through Use of an Additional Intra Cavity  
Low Bandwidth Gain Medium



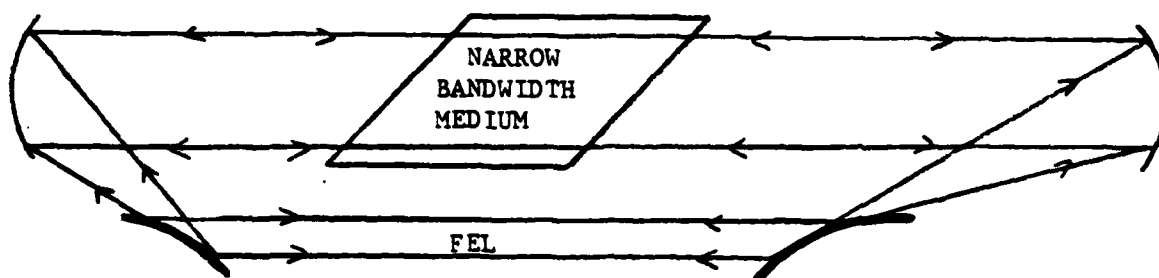


Figure 8. FEL Operation with an Additional Narrow Bandwidth Gain Region

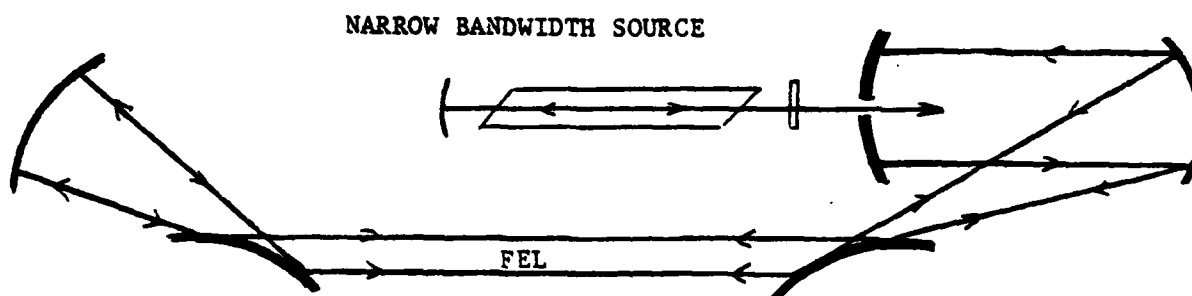


Figure 9. Injection Locking of FEL Cavity

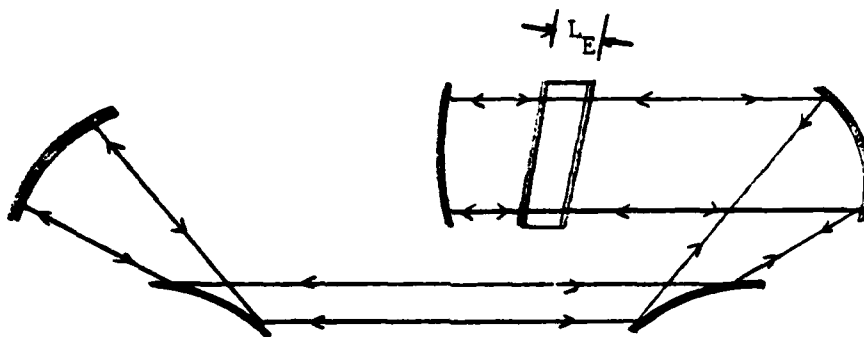
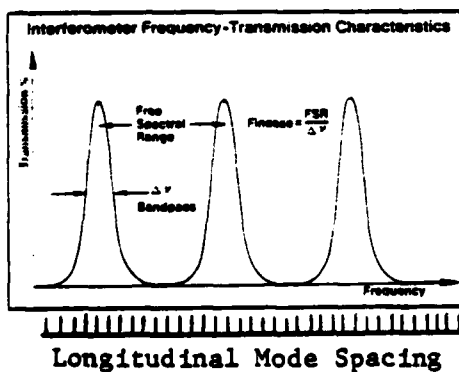


Figure 10. Use of a Fabry-Perot Etalon for SLM Selection



#### Useful Interferometer Definitions

Free Spectral Range:  $FSR = \frac{c}{2nL_E}$

Transmission:  $T = \frac{1}{n \left(1 - \frac{a}{t}\right)^2}$

Finesse:  $F = \frac{\pi \sqrt{F}}{n(1-r)}$

Bandpass:  $\Delta\nu = \frac{FSR}{F}$

$c$  = speed of light

$L_E$  = mirror spacing

$n$  = parameter

$n = 1$  for plane interferometer

$n = 2$  for confocal interferometer

Figure 11. Transmission of a Fabry-Perot Etalon

in Figure 11 along with a representation of the longitudinal mode pattern. The frequency spread between transmission peak, called the free spectral range, FSR, is given by  $c/2L_E$ . The FSR divided by the bandpass of each peak,  $\Delta\nu$ , is called the finesse of the etalon. Since there are  $\sim 100$  longitudinal modes within a gain bandwidth we require a finesse of  $\sim 100$  to select a SLM. To do this very high mirror, reflectivities in the etalon are required. Since  $F = \pi r^{1/2} (1-r)^{-1}$ , finesse of  $\sim 100$  requires mirror reflectivity,  $r = 97\%$ . The flux inside the etalon is increased by a factor of about  $(1-r)^{-1}$  or 33. Absorption and breakdown are likely problems for the FEL application.

Use of two finesse = 10 Fabry-Perot etalons, each with slightly different spacings, can be used to obtain an effective finesse of 100. The reflectivity of each element is 74% and the flux intensification is 3.8. Although the absorption and breakdown problems are reduced, they still exist, and the optical train is more complicated.

The sixth method of longitudinal mode selection is the use of a high resolution grating. There is no problem obtaining sufficient angular dispersion to select a single mode. However, the grating must be capable of resolving a single longitudinal mode of width  $\Delta\nu = c/2L \sim 1.5 \times 10^7$  to  $5 \times 10^7$  Hz over a frequency range of  $100 \times 10^9$  to  $1000 \times 10^9$  Hz. Thus the resolving power  $\nu/\Delta\nu = \lambda/\Delta\lambda = MN$  must be in the range 2,000 to 67,000, where N is the number of lines in the grating and M is the order of the grating. The lower resolving power, 2000, is for 100 GHz or 3mm wavelength 3 meter long cavities and the higher resolving power is for 1000 GHz or 0.3mm wavelength 10 meter long cavities. To minimize the size of the grating it should be in the form of an echelon

used at the Littrow angle (angle of incidence equals angle of reflection). This configuration is shown in Figure 12. The step size in the direction of light is  $\lambda/2$ . Only the first order exists. Thus the total length of the echelon in the optical direction for 2000 lines at 100 GHz (3mm) is  $2000 \times 1.5 = 3000 \text{ mm} = 3.0 \text{ meters}$ . For 67,000 lines at 1000 GHz (0.3mm) the length of the echelon is  $67,000 \times 0.15 = 10,000 \text{ mm} = 10 \text{ meters}$ . For a reasonable size optical beam cross-section, perhaps 20 x 20 cm, the step size perpendicular to the optical axis for the 2000 line echelon is 0.1mm and for the 67,000 line echelon is 3  $\mu\text{m}$ . Figure 13 shows a drawing of the etalon. We are not aware of an existing method of fabrication of echelons of the required 3-10 meter lengths. Alternative methods are stacking plates or ruling substrates or diamond machining of steps. Only the latter method seems possible in principle.

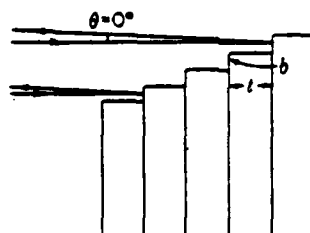


Figure 12. Reflection Echelon Used at Littrow Angle

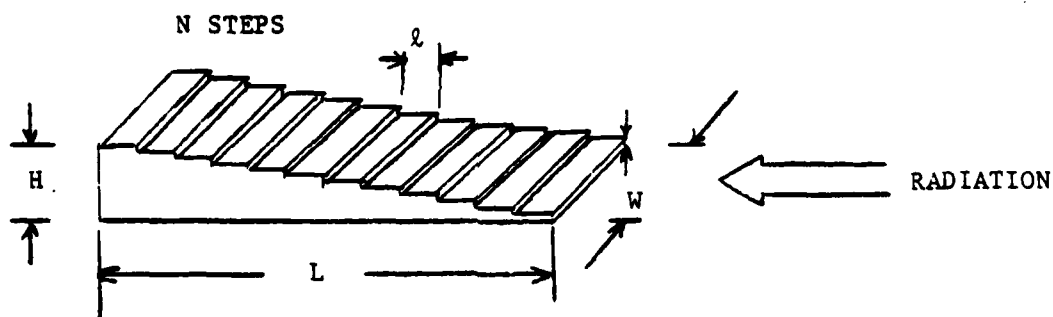


FIGURE 13. ECHELON USED FOR FEL.  $W \sim H \sim 20$  CM. RANGE OF VALUES FOR OTHER QUANTITIES IS (1)  $N = 2000$  STEPS,  $h = 0.1$  mm,  $l = 1.5$   $\mu$ m,  $L = 3$  METERS TO (2)  $N = 67,000$  STEPS,  $h = 3$   $\mu$ m,  $l = 0.15$  mm,  $L = 10$  METERS

SINCE CAVITY MODE SPACING  $= \Delta\nu = c/2L$ , RESOLVING POWER  $= \nu/\Delta\nu = N$  and GRATING SPACING  $= \lambda/2 = L_{\text{ETALON}}/N$ . THEN IT IS EASY TO SHOW THAT  $L_{\text{CAVITY}} = L_{\text{ETALON}}$ .

## VI. AXIAL FIELD GRADIENT BY INDUCTION

With the magnetostatic wiggler one could improve the single pass efficiency by varying the parameters of the wiggler in such a way that the ponderomotive potential well in which the electrons move is decelerated, thereby decelerating the electrons. In a magnetic wiggler both the period as well as the wiggler magnetic vector potential can be designed to vary in a prescribed manner. However, with an electromagnetic pump of wavelengths less than 1 mm, first, the pump vector potential is too small to contribute significantly to the resonance condition; and secondly, it is not possible to change the wavelength of the pump. It has been suggested that the electron beam can be made to interact at varying interaction angles to the pump radiation such that the effective pump wavelength is altered. Such a scheme, though attractive, would restrict the interaction length. An alternate scheme is to use an axial accelerating field to keep the electrons at resonant energy and to keep them trapped in the ponderomotive potential well. Purely electrostatic methods of applying the axial electric field are possible. These are not uniform to assure that the electrons will remain trapped over the entire interaction length. For pulsed machines it is possible to set up the axial field by induction. In this section we describe the basic design of an induction cell to provide such an acceleration to the electrons to enhance the energy recovery. Basic design considerations for the ferromagnetic accelerator cells have been sketched out by Birx and Wilson.<sup>13</sup> Reproduced below are some of the

considerations that were discussed by Birx and Wilson in the cited reference. The design factors that are important are:

"(1) The total core cross sectional area for induction.

The cross sectional area A is given by:

$$A = \int_0^{\tau} V dt / f \Delta B_s \quad (24)$$

where V is the accelerating-drive voltage,  $\tau$  the pulse length,  $\Delta B_s$  is the total flux swing available in the ferromagnetic material, f is the packing factor of the core. For metglass and other ferrite materials  $\Delta B_s$  is  $\sim 3T$ . As the pulse length increases for a given accelerating drive voltage, the cross sectional area of the core increases linearly or alternatively for a given cross section the accelerating drive voltage decreases inversely with the pulse length. Figure 14 gives the field gradient that can be obtained using metglass core.

(2) Core Losses:

The losses in the core material are directly proportional to the core volume which is given by

$$v = A\pi (R_o + R_i) \quad (25)$$

where  $R_o$  and  $r_i$  are the outer and inner radii of the core respectively. The losses results primarily from the low frequency B.H losses and the eddy currents. The resistivity of the ferrites is so high that the eddy current losses can be neglected. But for short pulses in the metallic ferromagnetic materials the eddy current losses dominate all other loss mechanism. Approximate values for the loss in joules per cubic meter are presented in Figure 15."

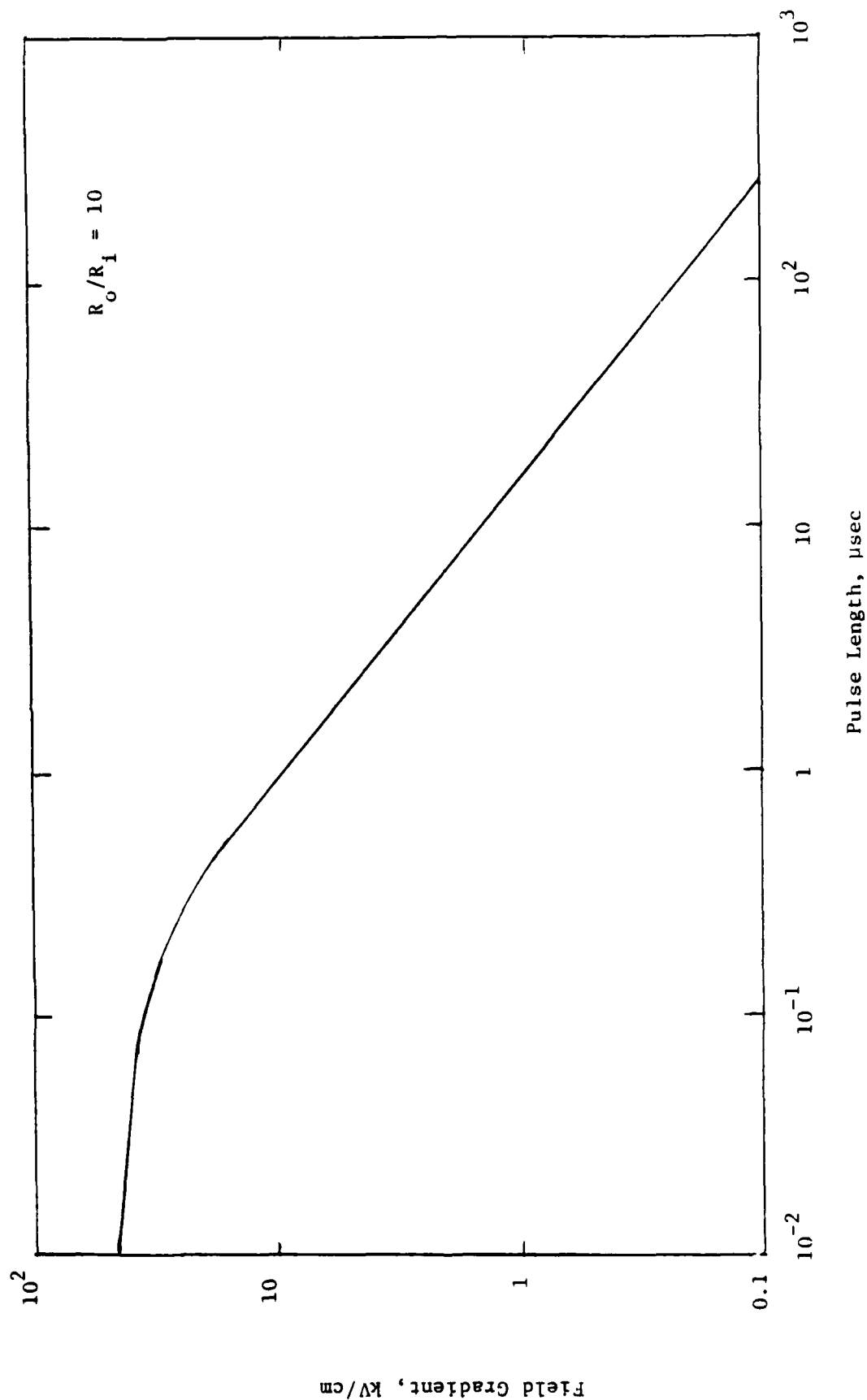


Figure 14. Practical Field Gradients that can be Obtained Using Metglass Core (From Ref. 13)



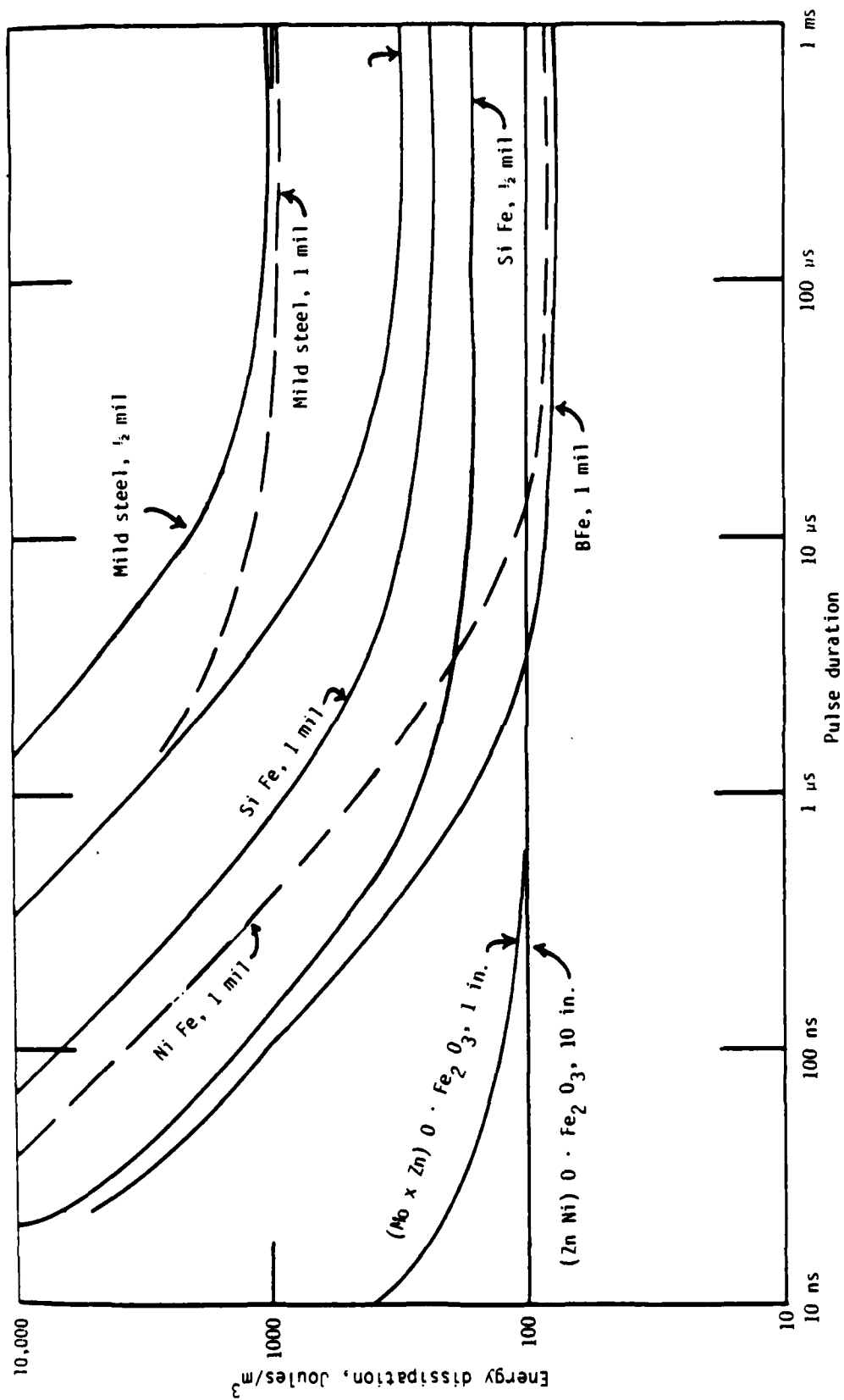


Figure 15. Energy Dissipation in Different Core Materials (From Ref. 13)

The accelerating gradient for the induction machines also becomes a concern for long pulses. As was mentioned earlier, the gradient is inversely proportional to the pulse length. The filling factor of the core along the beam line also has some practical limitations. Table IV represents data for losses and accelerating gradient in tabular form. Estimates of reasonable filling factors have been incorporated in the column giving overall accelerating gradient. The table has been taken from Ref. 13. The above analysis and tabulated results have been based upon the assumption that the entire volume of core material saturates simultaneously at the end of the pulse. However as the core outer radius increases and the inner radius remains relatively small, the inner regions of the core begin to saturate well before the outside regions. The eddy current losses will then begin to increase dramatically. One way to avoid this problem is by radial stacking of the cores to provide for more simultaneous saturation. In pulsed induction accelerators, the other important issue is resetting the core before the next electron pulse enters the wiggler. This has been discussed in detail in Ref. 13.

TABLE IV  
THE PREDICTED PROPERTIES OF VARIOUS CORE MATERIALS AND GEOMETRIES FOR  
SEVERAL PULSE DURATIONS (FROM REF. 13)

Material	$\tau$	( $\mu\text{m-cm}$ ) $\mu$	$\Delta B_5$	(m) $R_0$	$R_0$ $R_1$	$f$	Volume ( $\text{m}^3/\text{V}$ )	Weight ( $\text{g/V}$ )	Loss ( $\text{J/m}^3$ )	Loss ( $\text{J/V}$ )	V/m ( $\text{matl}$ )	V/m ( $\text{acc}$ )
Metglass 1 mil	50 ns	150	2.8	0.25	2	0.75	$2.8 \times 10^{-8}$	$1.54 \times 10^{-1}$	$2 \times 10^3$	$5.6 \times 10^{-5}$	$10.5 \times 10^{+6} \times 30\% = 3.5 \times 10^6$	
1/2 mil		150	2.8				$2.8 \times 10^{-8}$	$1.54 \times 10^{-1}$	$5 \times 10^2$	$1.4 \times 10^{-5}$	$10.5 \times 10^{+6}$	$3.5 \times 10^6$
NiFe 1 mil		50	2.4				$3.3 \times 10^{-8}$	$1.82 \times 10^{-1}$	$7 \times 10^3$	$23.0 \times 10^{-5}$	$9.0 \times 10^{+6}$	$3.0 \times 10^6$
1/2 mil		50	2.4				$3.3 \times 10^{-8}$	$1.82 \times 10^{-1}$	$1.7 \times 10^3$	$5.6 \times 10^{-5}$	$9.0 \times 10^{+6}$	$3.0 \times 10^6$
SiFe 2 mil		50	3				$2.6 \times 10^{-8}$	$1.43 \times 10^{-1}$	$32 \times 10^3$	$83.0 \times 10^{-5}$	$11.3 \times 10^{+6}$	$3.8 \times 10^6$
(ZnNi)OFe <sub>2</sub> O <sub>3</sub>		10"	0.5			1.0	$15.7 \times 10^{-8}$	$8.6 \times 10^{-1}$	$1 \times 10^2$	$1.6 \times 10^{-5}$	$1.9 \times 10^{+6} \times 50\% = 1.0 \times 10^6$	
Metglass 1 mil	100 ns	150	2.8	0.25	2	0.75	$5.6 \times 10^{-8}$	0.308	$1 \times 10^3$	$5.6 \times 10^{-5}$	$5.3 \times 10^6 \times 30\% = 1.6 \times 10^6$	
1/2 mil		150	2.8				$5.6 \times 10^{-8}$	0.308	$0.3 \times 10^3$	$1.7 \times 10^{-5}$	$5.3 \times 10^6$	$1.6 \times 10^6$
NiFe 1 mil		50	2.4				$6.6 \times 10^{-8}$	0.364	$4 \times 10^3$	$26 \times 10^{-5}$	$4.5 \times 10^6$	$1.4 \times 10^6$
1/2 mil		50	2.4				$6.6 \times 10^{-8}$	0.364	$1 \times 10^3$	$6.6 \times 10^{-5}$	$4.5 \times 10^6$	$1.4 \times 10^6$
SiFe 2 mil		50	3				$5.2 \times 10^{-8}$	0.286	$18 \times 10^3$	$93.6 \times 10^{-5}$	$5.7 \times 10^6$	$1.9 \times 10^6$
(ZnNi)OFe <sub>2</sub> O <sub>3</sub>		10"	0.5			1.0	$31 \times 10^{-8}$	1.72	$0.1 \times 10^3$	$3.1 \times 10^{-5}$	$1.0 \times 10^6 \times 50\% = 0.5 \times 10^6$	
Metglass 1 mil	1 $\mu\text{s}$	150	2.8	0.25	2	0.75	$5.6 \times 10^{-7}$	3.08	$1.7 \times 10^2$	$9.5 \times 10^{-5}$	$0.55 \times 10^6 \times 50\% = 0.27 \times 10^6$	
1/2 mil		150	2.8				$5.6 \times 10^{-7}$	3.08	$1 \times 10^2$	$5.6 \times 10^{-5}$	$0.53 \times 10^6$	$0.27 \times 10^6$
NiFe 1 mil		50	2.4				$6.6 \times 10^{-7}$	3.64	$4.5 \times 10^2$	$29.7 \times 10^{-5}$	$0.45 \times 10^6$	$0.23 \times 10^6$
1/2 mil		50	2.4				$6.6 \times 10^{-7}$	3.64	$1.7 \times 10^2$	$11.2 \times 10^{-5}$	$0.45 \times 10^6$	$0.23 \times 10^6$
SiFe 2 mil		50	3				$5.2 \times 10^{-7}$	2.86	$1.9 \times 10^3$	$99 \times 10^{-5}$	$0.57 \times 10^6$	$0.29 \times 10^6$
(ZnNi)OFe <sub>2</sub> O <sub>3</sub>		10"	0.5			1.0	$3.1 \times 10^{-6}$	17.2	$1 \times 10^2$	$31 \times 10^{-5}$	$0.10 \times 10^6$	$0.05 \times 10^6$
Metglass 1 mil	10 $\mu\text{s}$	150	2.8	0.25	2	0.75	$5.6 \times 10^{-6}$	30.8	$8 \times 10^1$	$44.8 \times 10^{-5}$	$0.053 \times 10^6 \times 75\% = 40 \times 10^3$	
1/2 mil		150	2.8				$5.6 \times 10^{-6}$	30.8	$8 \times 10^1$	$44.8 \times 10^{-5}$	$0.053 \times 10^6$	$40 \times 10^3$
NiFe 1 mil		50	2.4				$6.6 \times 10^{-6}$	36.4	$12 \times 10^1$	$79 \times 10^{-5}$	$0.045 \times 10^6$	$34 \times 10^3$
1/2 mil		50	2.4				$6.6 \times 10^{-6}$	36.4	$9 \times 10^1$	$59 \times 10^{-5}$	$0.045 \times 10^6$	$34 \times 10^3$
SiFe 2 mil		50	3				$5.2 \times 10^{-6}$	28.6	$16 \times 10^1$	$83 \times 10^{-5}$	$0.057 \times 10^6$	$43 \times 10^3$
(ZnNi)OFe <sub>2</sub> O <sub>3</sub>		10"	0.5			1.0	$3.1 \times 10^{-5}$	172	$1 \times 10^2$	$310 \times 10^{-5}$	$0.010 \times 10^6$	$7.5 \times 10^6$
Metglass 1 mil	1 $\mu\text{s}$				1.0	10	$16.4 \times 10^{-7}$	9.2	$1.7 \times 10^2$	$27.2 \times 10^{-5}$	$1.89 \times 10^6 \times 50\% = 0.95 \times 10^6$	
1/2 mil							$16.4 \times 10^{-7}$	9.2	$1 \times 10^2$	$16.4 \times 10^{-5}$	$1.89 \times 10^6$	$0.95 \times 10^6$
NiFe 1 mil							$1.94 \times 10^{-6}$	10.7	$4.5 \times 10^2$	$87.3 \times 10^{-5}$	$1.62 \times 10^6$	$0.8 \times 10^6$
1/2 mil							$1.94 \times 10^{-6}$	10.7	$1.7 \times 10^2$	$33 \times 10^{-5}$	$1.62 \times 10^6$	$0.8 \times 10^6$
SiFe 2 mil							$1.53 \times 10^{-6}$	8.4	$1.9 \times 10^3$	$290 \times 10^{-5}$	$2.03 \times 10^6$	$1.01 \times 10^6$
(ZnNi)OFe <sub>2</sub> O <sub>3</sub>						1.0	$9.1 \times 10^{-6}$	50	$1 \times 10^2$	$91 \times 10^{-5}$	$0.34 \times 10^6$	$0.17 \times 10^6$
Metglass 1 mil	10 $\mu\text{s}$					0.75	$1.64 \times 10^{-5}$	92	$8 \times 10^1$	$131 \times 10^{-5}$	$0.19 \times 10^6 \times 75\% = 0.142 \times 10^6$	
1/2 mil							$1.64 \times 10^{-5}$	92	$8 \times 10^1$	$131 \times 10^{-5}$	$0.19 \times 10^6$	$0.142 \times 10^6$
NiFe 1 mil							$1.94 \times 10^{-5}$	107	$12 \times 10^1$	$232 \times 10^{-5}$	$0.16 \times 10^6$	$0.121 \times 10^6$
1/2 mil							$1.94 \times 10^{-5}$	107	$9 \times 10^1$	$174 \times 10^{-5}$	$0.16 \times 10^6$	$0.121 \times 10^6$
SiFe 2 mil							$1.53 \times 10^{-5}$	84	$16 \times 10^1$	$244 \times 10^{-5}$	$0.20 \times 10^6$	$0.152 \times 10^6$
(ZnNi)OFe <sub>2</sub> O <sub>3</sub>						1.0	$9.1 \times 10^{-5}$	500	$1 \times 10^2$	$910 \times 10^{-5}$	$0.03 \times 10^6$	$0.025 \times 10^6$

## VII. REFERENCES

1. S. A. Mani, "Low Voltage Free Electron Laser" Volume II-Theory, WJSA-FTR-81-168, June 1981, prepared for Office of Naval Research under Contract No. N00014-80-C-0515.
2. S. A. Mani, "Low Voltage Free Electron Laser Optics," WJSA-FTR-82-193 (March 1982), prepared for Office of Naval Research under Contract No. N00014-80-C-0515.
3. S. A. Mani, "Low Voltage Free Electron Laser Optics - First Stage Design," WJSA-FTR-82-209 (November 1982), prepared for Office of Naval Research under Contract No. N00014-80-C-0515.
4. C. K. Carniglia and J. H. Apfel, J. Opt. Soc. Am. 70, 523 (1980).
5. Leo Young, J. Opt. Soc. Am. 52, 753 (1962).
6. G. Koppelman, Ann. Phys. (Leipzig) 5, 388 (1960).
7. George J. Simonis, Int. J. Infrared and Millimeter Waves, 2, 439 (1982).
8. J. R. Birch, J. D. Dromey and J. Lesurf, Infrared Physics 21, 225 (1981); National Physical Laboratory Report NPL-DES 69 (1981).

REFERENCES (CONTINUED)

9. D. R. Corson and P. Lorrain, "Introduction to Electromagnetic Fields and Waves," W. H. Freeman & Co., San Francisco (1962), pp. 332-404.
10. R. S. Longhurst, "Geometrical and Physical Optics," Longman Publishers, London (1967), pp. 465-477.
11. A. Girard, Optics Communications 11, (1974).
12. Izatt et al. IEEE J.Q.E. 13, 396 (1977).
13. D. Birk and M. Wilson in the "Proceedings of the First Joint DoE/DOD Accelerator Technology Workshop," September 15-19, 1980, W. J. Schafer Associates, Inc. Report WJSA-LJ-80-32 (1980).



